LITHO1.0: AN UPDATED CRUST AND LITHOSPHERE MODEL OF THE EARTH

T. Guy Masters[1], Zhitu Ma[1], Gabi Laske[1], and Mike Pasyanos[2]

University of California San Diego[1] and Lawrence Livermore National Laboratory[2]

Sponsored by the Air Force Research Laboratory

Award Nos. FA8718-09C-0008 and DE-AC52-07NA27344
Proposal No. BAA09-32

ABSTRACT

We are developing LITHO1.0: an updated crust and lithosphere model of the Earth. The overall plan is to take the popular CRUST2.0 model—a global model of crustal structure with a relatively poor representation of the uppermost mantle—and improve its nominal resolution to 1 degree and extend the model to include lithospheric structure. The new model, LITHO1.0, will be constrained by many different datasets, including extremely large new datasets of relatively short-period group velocity data measured with a new technique which are sensitive to lid properties as well as crustal thickness and average crustal properties. Other datasets include (but are not limited to) compilations of receiver function constraints and active source studies.

This year, most progress was made on surface-wave measurements. We use a cluster analysis technique to measure surface-wave group velocity from 10mHz to 40mHz . We use all the LH data from the Data Management Center (DMC) of Incorporated Research Institutions for Seismology (IRIS) between 1976 and 2007. The Rayleigh wave group velocity dataset is complete. The current dataset has about 330000 measurements for each of 10 mHz and 20mHz , 210000 for 30mHz , and 45000 for 40mHz . We also include some BH data from Program for Array Seismic Studies of the Continental Lithosphere (PASSCAL) in the southern hemisphere and the Portable Observatories for Lithospheric Analysis and Research Investigating Seismicity (POLARIS) network to increase ray coverage. Initial inversions of the datasets show features consistent with geophysical observation. Some artifacts are found in the ocean regions at high frequencies due to limited ray coverage. A solution we are currently pursuing is to implement an a priori group velocity model based on the age of oceanic lithosphere, which will be used to constrain the inversions where necessary.

We anticipate the new model will provide a much more accurate representation of regional phases, including the propagation of Pn and Sn phases, which strongly depend on lid structure. The new model will also provide a good starting point for more-accurate regional models using specialized datasets that can then be naturally embedded in a global model.

OBJECTIVES

The main objective is to take the popular CRUST2.0 model—a global model of crustal structure with a relatively poor representation of the uppermost mantle—and improve its nominal resolution to 1 degree and extend the model to include lithospheric structure. The new model, LITHO1.0, will be constrained by many different datasets, including extremely large new datasets of relatively short-period group velocity data measured with a new technique, which are sensitive to lid properties as well as crustal thickness and average crustal properties. Other datasets include (but are not limited to) compilations of receiver function constraints and active source studies.

RESEARCH ACCOMPLISHED

Global Surface Wave Group Velocity Datasets

Surface-wave group velocity measurements have been made for many decades, and most algorithms are based on the one first introduced by Dziewonski et al. (1969), which uses a suite of Gaussian narrow pass-band filters to generate a set of frequency-dependent envelope functions. The group arrival time is taken to be the peak of the envelope function. Further developments of this technique are described in Levshin et al. (1992), which introduces some interactive techniques to improve the measurements (see also Keilis-Borok, 1989). Levshin and co-workers have made many such measurements, and these have been used in both regional (Ritwoller and Levshin, 1998; Ritzwoller et al., 2001; Villasenor et al., 2001; Levshin et al., 2001) and global (Ritzwoller et al, 2002; Shapiro and Ritzwoller, 2002) inversions for group velocity maps and near-surface structures. The interactive nature of this algorithm makes construction of large datasets very time consuming, though the recent global analyses have about 100,000 measurements per frequency (Ritzwoller et al., 2002).

Here, we describe a different technique to measure the relative group arrival times of surface wave packets, which allows very efficient construction of large data sets. We have applied the technique to all LH data at the IRIS DMC from events larger than Ms = 5.5 between 1976 and 2007. We also include some BH data from PASSCAL experiments in the southern hemisphere and the POLARIS network to increase ray coverage. The Rayleigh wave group velocity data set is complete from 10mHz to 40mHz. The current data set has about 330000 measurements for each of 10mHz and 20mHz, 210000 for 30mHz, and 45000 for 40mHz. We have also performed a ray-theoretical inversion of the data for group velocity perturbation maps to allow us to estimate the internal consistency of the data. The data are surprisingly well fit by this simple inversion even though, as previously shown (e.g., Ritzwoller and Levshin, 1998), perturbations in group velocity reach 30% at 50 seconds and are bigger at shorter periods. Similar datasets for Love waves are under construction and are complete for data through 2005.□□

Our method starts in a similar fashion to the traditional group velocity measurement in that we apply a narrow-band Gaussian filter to the data and compute the envelope function (after correcting to a common instrument response and for the source phase). The difference is that we choose only one pass band and compute the envelope functions of all records for an event. We then treat these envelope functions in the same way as we do body waveforms in our cluster-analysis technique (Reif et al., 2001, Houser et al., 2008).

The first hundred envelope functions for an event are plotted in Figure 1. The envelope functions are displayed centered on their predicted group arrival time and are ordered by distance. This example is for Rayleigh waves band-passed with a center frequency of 20mHz and a bandwidth of 5mHz . Note how similar to each other most of the envelope functions are, and while this particular sample has only a couple of examples, shifts in the envelope functions of over 200 seconds from the expected arrival times are not uncommon.

We consider all records in the distance range of 20 to 160 degrees, though waveforms tend to be distorted for short-period waves propagating long distances. Measurements are made interactively, and the user first picks a desired time window for cross-correlation. Cross-correlation functions for every trace with every other trace are computed using a time domain method, and the (positive) peaks in the cross-correlation function that contain the differential time and scaling information between the traces are identified. Using cluster analysis (e.g., Hartigan, 1975), the stations are sorted by the similarity of their waveforms, and a cluster tree is plotted that shows at what level of correlation the various groups may be joined. The user then selects a minimum correlation coefficient to use as a cutoff for the cluster divisions. There is a tradeoff between having a large number of clusters with highly similar waveforms and a smaller number of clusters with less-correlated waveforms.

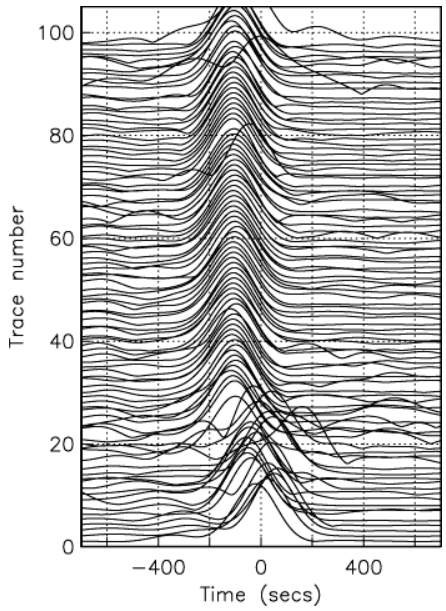

Figure 1. The first 100 envelope functions for an event on 2003:8, ordered by distance and aligned on the expected group arrival time. This example is for 50-second Rayleigh waves and demonstrates how similar envelope functions are, even though they occasionally are delayed by more than 200 seconds.

Optimal time shifts for the stations within each cluster are then obtained using a weighted least squares method that also returns error estimates based on the internal consistency of the time shifts (VanDecar and Crosson, 1990). These error estimates are often grossly optimistic, so we get an independent estimate of true errors using the consistency of group arrival times at closely spaced stations.

The clustering is illustrated in Figure 2. The left side shows the waveforms, which have been organized into clusters, the right hand side shows the cluster tree that governs the clustering. The user determines the degree of clustering with a vertical cursor (see figure caption).

Experiments with spherical-Earth synthetic waveforms suggest that envelope shape should correlate well at all distances and, in practice, many of the envelope functions for an event cross-correlate extremely well with each other, sometimes allowing over 200 relative group arrival times to be estimated simultaneously. Experiments with synthetic seismograms also show that the algorithm gives accurate, unbiased estimates of relative group arrival times. For events with variable waveforms (due to low signal, source directivity effects, overtone contamination, etc.), the clustering allows efficient isolation of those waveforms with simple envelope functions without prescreening of the data. This lack of need to prescreen the data is essential when dealing with very large datasets. It is important to note that we keep only those measurements for clusters with simple envelope shapes (about 20% of the data at long periods and less than 10% of the data at short periods). This may help explain why very simple ray-theory-based inversions of the data are extremely successful at explaining the measurements (see below)

When we compute the envelopes, we also measure the peak arrival time of the envelope and the centroid frequency of the spectrum. The relative arrival times are best fit to the measured peak arrival times to determine a set of absolute group arrival times. The centroid frequency is taken to be a better estimate of the frequency of the actual measurement than the center of the Gaussian filter (Shapiro and Singh, 1999) and varies from record to record. It is typically about 2% higher than the filter center.

Comparison with Previous Datasets

We compare the new dataset with another large, global group velocity dataset from the Colorado group (henceforth cub) though our current dataset (henceforth ucsd) is about a factor of 4 larger in size. The cub dataset was measured using traditional measurement techniques, and there was no correction for source phase that might account for some discrepancies at the longer periods (Levshin et al., 1999). At 20mHz , there are 330,000 ucsd measurements and about 85000 cub measurements, of which only 24,300 overlap.

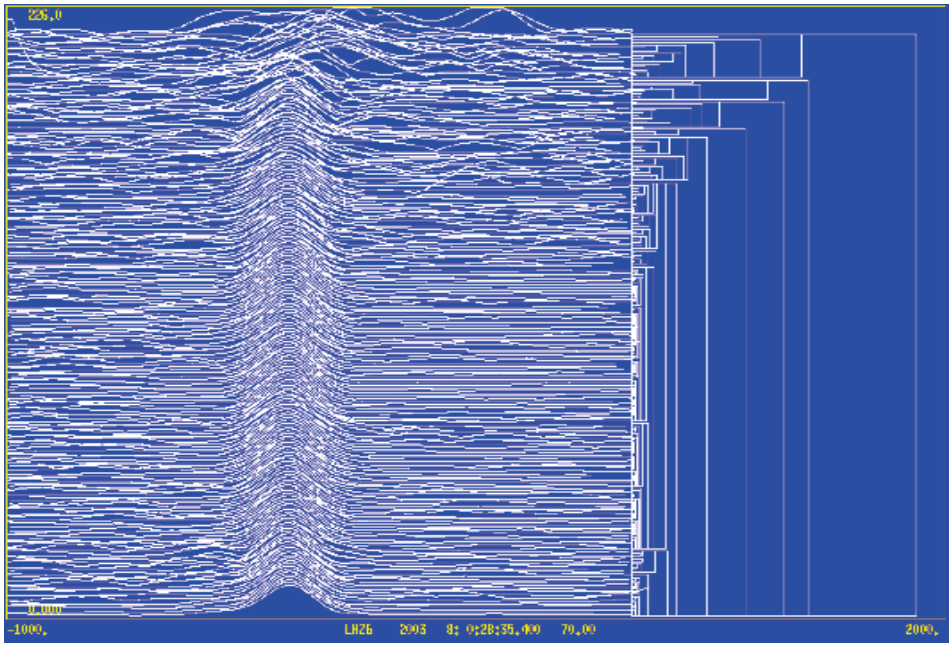

Figure 2. Screen capture of all envelope functions for 50-second Rayleigh waves between distances of 20 and 160 degrees for an event on 2003:8, after clustering. The left side shows the aligned traces sorted by degree of similarity into clusters. The tree diagram on the right allows the user to decide how finely clustering needs to be done. A vertical cursor is used to do this—as the cursor is moved to the left of the cluster tree plot, the waveforms are divided into smaller and smaller clusters. In this case, the cursor would be clicked close to the left, dividing the waveforms into one or two large clusters, leaving a group of uncorrelated traces near the top of the plot. Once the level of clustering has been chosen, the differential times between traces in each cluster are remeasured using cross correlation.

Since the precision of apparent group velocities is a strong function of distance, we compare group arrival times that are expected to be of similar precision regardless of distance. There are some uncertainties here because our measurements are each from slightly different frequencies while we believe that the cub group interpolates their group velocity curves to the desired frequency. However, the average offset between the two datasets is only 2 seconds, which is much smaller than our measurement precision.

The scaled median absolute deviation (SMAD) of the difference between group arrival time residuals is about 12 seconds. This is larger than we expected and about 50% larger than our inferred measurement precision at this frequency (about 7 seconds—obtained by looking at arrival times at nearby stations). This discrepancy is also bigger than the expected effect of including the source phase shift (from measurements on synthetics, we find that the source phase can lead to a time error of about 7 seconds at 10mHz and about 4 seconds at 20mHz). On the other hand, we should point out that the measurement discrepancy is much smaller than the signal in the actual data (Figure 3). Indeed, group velocity maps made using the two different datasets are extremely similar. The fact that there is no systematic difference between the datasets means that they can be combined in an inversion, and we find that maps made from the combined datasets fit both datasets almost as well as maps made from the separate datasets.

Estimation of Group Velocity Maps

To evaluate the internal consistency of our group arrival time measurements, we have performed a simple inversion, based on ray theory assuming great circle propagation. We discretize the Earth's surface into equal area cells of 1 or 2 degrees in dimension at the equator. Sampling of the Earth is quite nonuniform, though most cells have more than 500 hits, and all cells have more than 100 hits (Figure 4). Some cells in the western U.S. have over 10,000 hits, suggesting that more-sophisticated inversions could use a finer parameterization in this region or one using a variable tessellation, as is used in other tomographic inversions. Coverage in most of Eurasia is excellent.

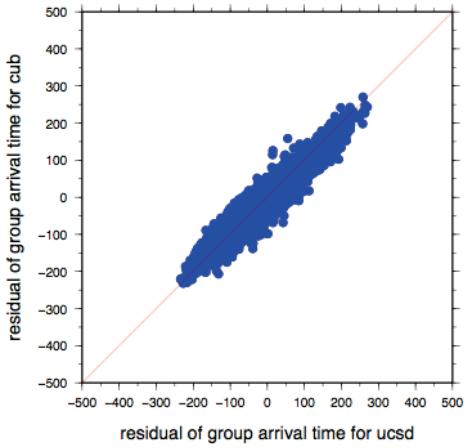

Figure 3. Scatter plot of the residual of group arrival time for ucsd and cub data set at 20 mHz .

The data are inverted using LSQR (Paige and Saunders, 1982) with a light smoothing constraint on the first lateral derivative of structure. Convergence is fast, reflecting the well-conditioned nature of the inversion. The resulting maps (Figure 5) are similar to the global maps of Shapiro and Ritzwoller (2002) or the regional maps of Ritzwoller and Levshin (1998) but show more detail and higher amplitudes. We suspect this is because the greater number of data used here means that less smoothing is required.

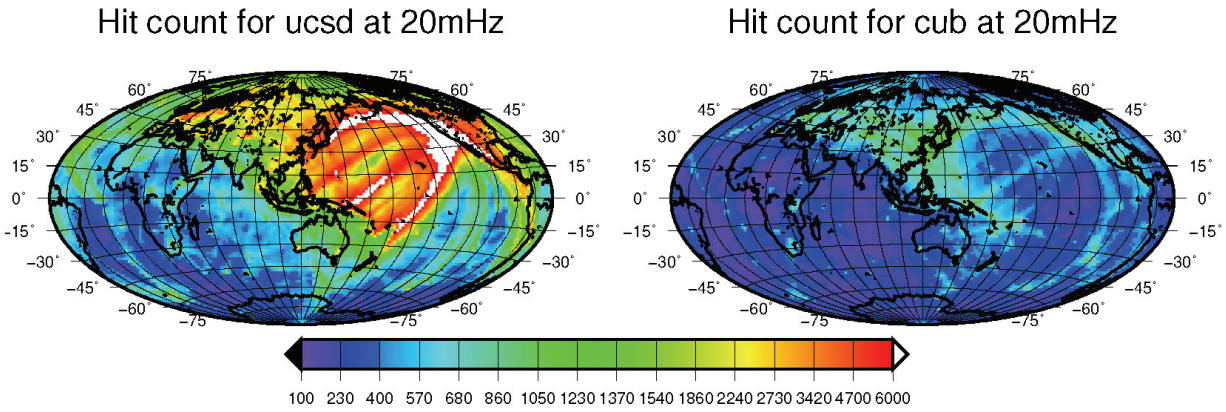

Figure 4. Hit count for the ucsd and cub datasets. Notice that all cells have more than 100 hits for both datasets, though the cub dataset focuses more on Eurasia.

Consider the map at 20mHz . Clearly, the biggest signal in continental regions is due to variations in crustal thickness. Most extreme group velocity variations occur under Tibet (30%) and under the Andes. This is not surprising since the sensitivity of 50-second Rayleigh waves peaks at 70–100 km, so we are actually seeing a crust-mantle signal. Other continental signals seem associated with hot spots (East Africa). The signal in oceanic regions is also interesting, with extremely slow regions associated with back-arc basins (e.g., the Lau basin) and some hot spots (e.g., Galapagos) but not others (Iceland, Hawaii). Some parts of the East Pacific Rise are clearly very slow, and there is a perceptible slow anomaly associated with the Australian-Antarctic discordance.

Currently, we have produced Rayleigh wave group velocity maps between 10mHz and 40mHz at frequency increments of 2.5mHz. These maps are extremely good representations of the group arrival time data, typically giving variance reductions of well over 90% (Figure 6). In some ways, this is surprising since we are using a very simple theory to model the data, and we have performed many tests to detect possible biases. These include using finite frequency kernels (Dahlen and Zhou, 2006) for the longer periods (Masters et al, 2005, 2006), doing surface wave ray tracing at shorter periods to check the effect of large velocity perturbations, making measurements from SEM synthetics and inverting them in a variety of ways, etc. Surprisingly, simple great-circle ray theory is usually

adequate—possibly because our measurement technique selects only those surface wave packets whose envelopes are simple in shape.

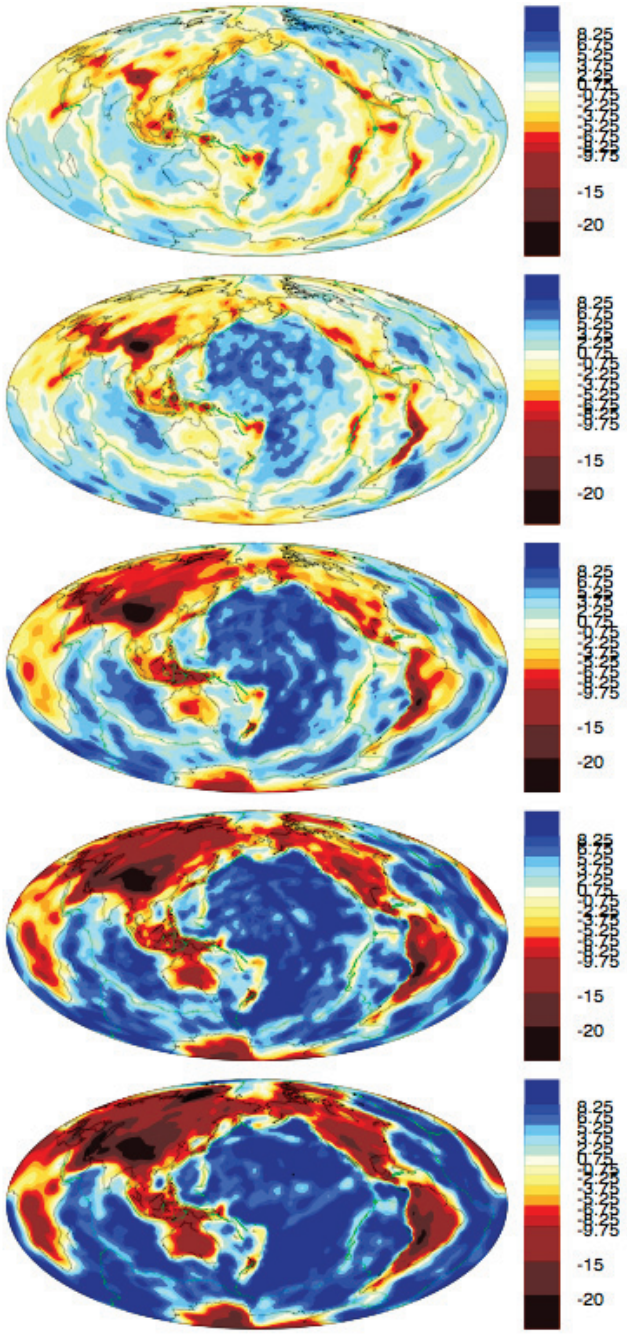

Figure 5. Group velocity perturbation maps at frequencies, from top to bottom, 15mHz, 20mHz, 25 mHz, 30mHz, and 35mHz.

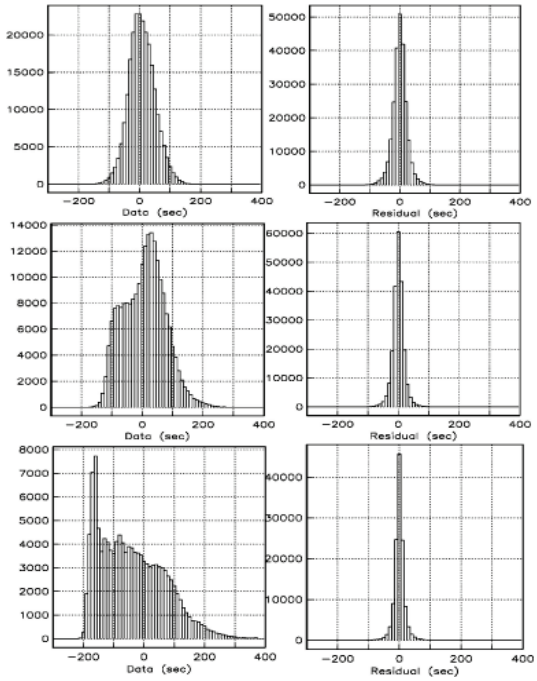

Figure 6. Histograms of group arrival time residuals before and after inversion. Top: 10mHz, variance reduction is 76%; middle 20mHz, variance reduction is 94%; bottom 30mHz, variance reduction is 98%.

Constraining Group Velocity Maps Using Physical Models

In recent years, there have been several attempts to relate seismic data directly to the parameters of a physical model (e.g., Goes et al., 2000; Cammarano et al., 2003; Shapiro and Ritzwoller, 2004). While there is no "simple theory" of continental structure, the half-space cooling model of oceanic lithosphere and its variants suggest that we might be able to predict group velocities in oceanic regions quite accurately. We are motivated to include such physical models because, at short periods, group velocity measurements are difficult to make for long paths, with the result that several parts of the ocean basins are not well constrained.

When the maps shown in Figure 5 are binned by oceanic lithospheric age, they produce quite simple variations of group velocity with age up to about 120Ma. Older regions show much greater variability, particularly at short periods, where the group velocity tends to be lower than expected (Figure 7). This suggests that thermal rejuvenation of old oceanic lithosphere is quite common, but it also suggests that a physical model could be successful up to ages of about 120Ma. Several attempts to predict oceanic structure as a function of lithospheric age have been made, with perhaps the most-sophisticated thermodynamic models being those of Stixrude and Lithgow-Bertelloni (2005). Some of these studies (e.g., Shapiro and Ritzwoller, 2004) have had to resort to introducing a baseline shift so that the physical models predict group velocities in accordance with those shown in Figure 7. We find this to be rather unsatisfactory. The models of Stixrude and Lithgow-Bertelloni (2005) also show complex structure in the lid due to phase transitions in feldspar and spinel (using a pyrolite composition). There is no seismic evidence for such complex structure, which would be consistent with the likely scenario that the uppermost mantle is depleted. We therefore parameterize our model with a crust (taken from CRUST2.0), which we take to first order to be independent of age. With careful attention to physical dispersion effects (since Q in the asthenosphere is very low), we modified the QL6 attenuation model (Durek and Ekstrom, 1996) and find that a model based on pyrolite and a cooling half-space thermal profile (Figure 8) can reproduce the data in Figure 7 quite well.

The Q value in our model at 100km depth is very close to other Q models, such as Romanowicz (1996), but the predicted attenuation for surface waves is stronger than the model from Dalton and Ekstrom (2006). While these results are preliminary (e.g., future models will take account of what we know about Pn and Sn in ocean basins and allow for variations in lid structure), they do suggest that the models can provide a basis for constraining inversions at the shorter periods, where the unconstrained inversions are less precise.

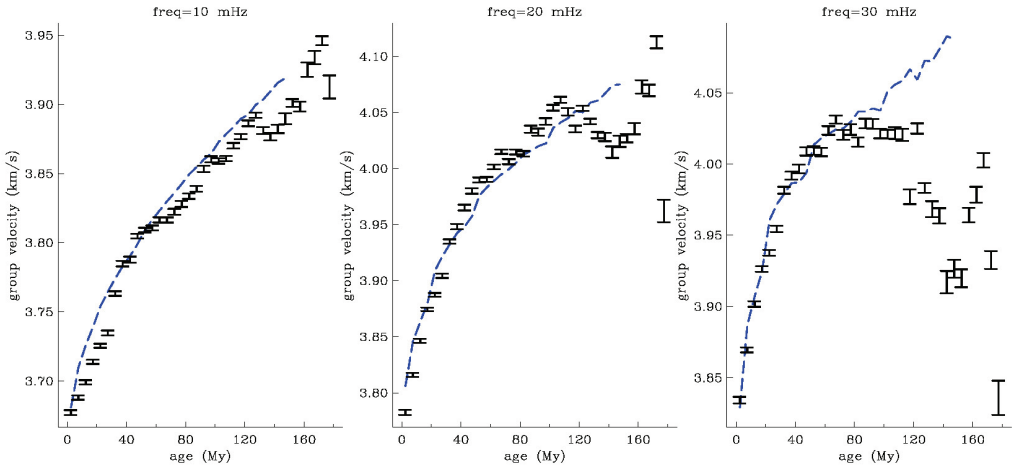

Figure 7. Group velocity maps binned by lithosphere age for 10, 20, and 30mHz. The error bars indicate the standard deviation of the mean of each bin. The dashed line shows the predicted group velocity from our physical model with a modified QL6 attenuation model.

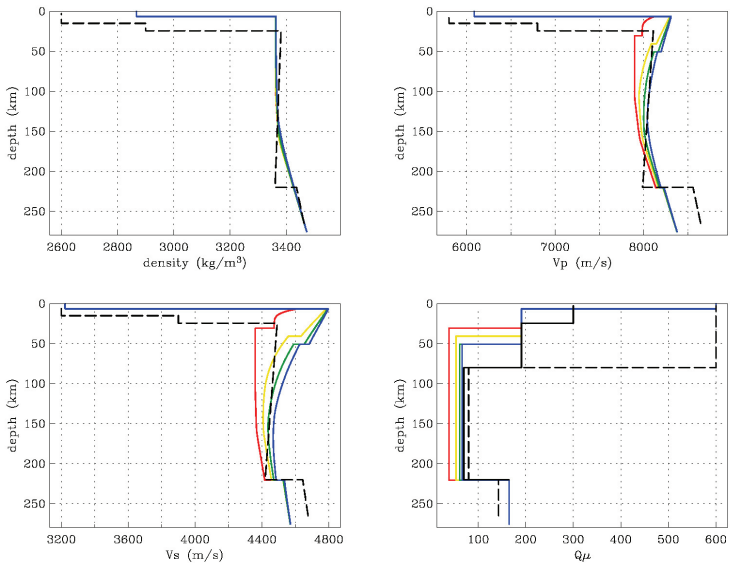

Figure 8. Vp,Vs, density, and Q models that produce the group velocity shown in Figure 7. Colored lines show depth profiles for different ages (Red: 1My, Yellow: 50My, Green: 100My, Blue: 150My). The dashed line is the PREM model. The solid black line in the plot of Q value is the QL6 model.

CONCLUSIONS AND RECOMMENDATIONS

We have completed the construction of a new large global dataset of Rayleigh wave group arrival times using a new efficient measurement technique and have evaluated the data by constructing group velocity maps using simple ray theory.

Comparisons of the data with datasets of previous workers show no bias in the data, but measurement discrepancies are about 50% larger than we would expect, based on estimates of precision of the measurements. While part of this discrepancy can be ascribed to source effects, we are uncertain what causes the remainder of the discrepancy. The measurement discrepancies are much smaller than the signal in the data, and the group velocity maps that we generate are capable of explaining almost all the signal in the data.

At short periods, we find that parts of the ocean basins are not well sampled, and we use the longer-period data to construct a physical model of oceanic structure that accurately predicts the age dependence of group velocity out to about 120Ma. Such models can be used as loose constraints on the short-period inversions. They can also be used to identify and evaluate apparent deviations in group velocity from the basic physical model.

The next step in this project is to finalize the group velocity maps and do a formal resolution and error analysis at each period. We have recently adapted the technique to vary the Gaussian filter until the centroid frequency for each spectrum matches the target frequency. Preliminary results show that the refinement makes very little difference to the final maps.

We are also close to completing the equivalent dataset for Love waves, which will be subject to the same analysis described above.

ACKNOWLEDGEMENTS

The data used in this research is obtained from IRIS Data Management Center and Canadian National Seismograph Network. We thank M. H. Ritzwoller and A. L. Levshin for personal communications.

REFERENCES

Cammarano, F., S. Goes, P. Vacher, and D. Giardini (2003). Inferring upper-mantle temperatures from seismic velocities, *Phys. Earth Planet. Int*. 138: 197–222.

Dahlen, F. A. and Y. Zhou (2006). Surface wave group delay and attenuation kernels, *Geophys. J. Int.* 165: 545–554.

Dalton, C. A. and G. Ekstrom (2006). Global models of surface wave attenuation, *J. Geophys. Res.* 111: B05317, doi:10.1029/2005JB003997.

Dziewonski, A. M., S. Bloch, and M. Landisman (1969). A technique for the analysis of transient seismic signals, *Bull. Seism. Soc. Am*. 59: 427–444.

Durek, J. and G. Ekstrom (1996). A radial model of anelasticity consistent with long-period surface-wave attenuation, *Bull. Seism. Soc. Am*. 86: 144–158.

Goes, S., R. Govers, and P. Vacher (2000). Shallow mantle temperatures under Europe from P and S wave tomography, *J. Geophys. Res*. 105: 11,153–11,169.

Hartigan, J. A. (1975). *Clustering Algorithms*. New York, NY: John Wiley & Sons, Inc.

Houser, C., G. Masters, P. Shearer, and G. Laske (2008). Shear and compressional velocity models of the mantle from cluster analysis of long-period waveforms, *Geophys. J. Int.* (in press).

Keilis-Borok, V. I., Ed. (1989). Seismic Surface Waves in Laterally Inhomogeneous Earth. Doredrecht, Neterlands: Kulwer.

Levshin, A., L. Ratnikova, and J. Berger (1992). Peculiarities of surface wave propagation across central Eurasia, *Bull. Seism. Soc. Am*. 82: 2464–2493.

Levshin, A. L., M. H. Ritzwoller, and J. Resovsky (1999). Source effects on surface wave group travel times and group velocity maps, *Phys. Earth Planet. Int*. 115: 293–312.

Levshin, A. L., M. H. Ritzwoller, M. P. Barmin, A. Villasenor, and C. A. Padgett (2001). New constraints on the Arctic crust and uppermost mantle: Surface wave group velocities, Pn, and Sn, *Phys. Earth Planet. Int*. 123: 185–204.

Masters, G., D. Kane, J. Morrow, Y. Zhou, and J. Tromp (2005). Measurement and interpretation of surface wave group arrival times, *EOS Trans. AGU* 86: fall meeting supplement; abstract S42A-05.□□

Masters, G., Y. Zhou, and J. Tromp (2006). Measurement and interpretation of surface wave group arrival times, *EOS Trans. AGU* 87: fall meeting supplement; abstract S54B-01.

Paige, C. C. and M. A. Saunders (1982). LSQR: An algorithm for sparse linear equations and sparse least squares, *TOMS* 8: 43–71. □□

Reif, C., G. Masters, G. Laske, P. Shearer, and M. Flanagan (2001). Joint inversions for velocity and discontinuity structure in the mantle, *EOS Trans. AGU* 82: F888, fall meeting supplement.□□

Ritzwoller, M. H. and A. L. Levshin (1998). Eurasian seismic tomography: Group velocities, *J. Geophys. Res*. 103: 4838–4878

Ritzwoller, M. H., N. M. Shapiro, A. L. Levshin, and G. M. Leahy (2001). The structure of the crust and upper mantle beneath Antarctica and the surrounding oceans, *J. Geophys. Res*. 106: 30645–30670.

Ritzwoller, M. H., N. M. Shapiro, M. P. Barmin, and A. L. Levshin (2002). Global surface wave diffraction tomography, *J. Geophys. Res*. 107: 2335.

Romanowicz, B. (1995). A global tomographic model of shear attenuation in the upper mantle, *J. Geophys. Res*. 100: 12,375–12,394.

Shapiro, N. M. and S. K. Singh (1999). A systematic error in estimating surface-wave group-velocity dispersion curves and a procedure for its correction, *Bull. Seism. Soc. Am*. 89: 1138–1142.

Shapiro, N. M. and M. H. Ritzwoller (2002). Monte-Carlo inversion for a global shear velocity model of the crust and upper mantle, *Geophys. J. Int*. 151: 88–105.

Shapiro, N. M. and M. H. Ritzwoller (2004). Thermodynamic constraints on seismic inversions, *Geophys. J. Int*. 157: 1175–1188.

Stixrude, L. and C. Lithgow-Bertelloni (2005). Mineralogy and elasticity of the oceanic upper mantle: Origin of the low-velocity zone, *J. Geophys. Res*. 110: B03204, doi:10.1029/2004JB002965.

VanDecar, J. C. and R .S. Crosson (1990). Determination of teleseismic relative phase arrival times using multi-channel cross correlation and least squares, *Bull. Seism. Soc. Am*. 80: 150–169.□□

Villasenor, A., M. H. Ritzwoller, A. L. Levshin, M. P. Barmin, E. R. Engdahl, W. Spakman, and J. Trampert (2001). Shear velocity structure of Central Eurasia from inversion of surface wave velocities, *Phys. Earth Planet. Int.* 123: 169–184.□□